Packed column dynamic studies and breakthrough curve analysis for adsorption of paraquat herbicide onto agroindustrial ashes

Manisha G. Kamble, Milind D. Nagrale, Ankit A. Kamdi, Sunil K. Deokar, Sachin A. Mandavgane*

Department of Chemical Engineering, Visvesvaraya National Institute of Technology, South Ambazari Road, Nagpur 440010, India, Tel. +91-712- 2801578, email: manisha6189@gmail.com (M.G. Kamble), milind.vnit@gmail.com (M.D. Nagrale), ankitkamdi@students.vnit.ac.in (A.A. Kamdi), Tel. +91-712- 2801650, email: sunildeokar.2008@gmail.com (S.K. Deokar), Tel. +91-712-2801563, Fax 91-712-2223969, email: mandavgane1@gmail.com (S.A. Mandavgane)

ABSTRACT

Adsorptive removal of paraquat from aqueous solution is performed in continuous mode using packed beds of RHA and BFA. The packed-bed parameters of RHA and BFA are determined and compared at different influent concentrations, flow rates, and bed heights. The maximum saturation capacity of RHA (6.96 mg/g) is found at 2 mL/min (flow rate) and 6.4 cm (bed height), whereas that of BFA (20.55 mg/g) is found at 5 mL/m in (flow rate) and 8.8 cm (bed height) for 20 mg/L (concentration). The volume of paraquat solution treated using RHA and BFA for the aforementioned experimental conditions is 2380 mL and 7800 mL, respectively. The bed saturation time and fractional bed utilization of BFA are higher than those of RHA. The bed depth service time (BDST), Thomas, and Yoon–Nelson models are applied to predict the behavior of breakthrough curves. The BDST model reveals the complex mechanism comprising more than one rate-limiting step for the adsorption of paraquat on RHA and BFA. The value of effluent concentration predicted by the Thomas model is in accordance with the experimental value. The lower value of standard deviation between the experimental and predicted times for 50% saturation indicates the applicability of the Yoon–Nelson model for packed-bed adsorption of paraquat on both RHA and BFA.

Keywords: Paraquat; Rice husk ash; Bagasse fly ash; Packed-bed model

1. Introduction

Contamination of surface waters and groundwaters due to increasing pollution has become a major ecological concern. Discharge of pesticides from various sources such as manufacturing plants, spraying, and accidental spills are one of the primary causes of water contamination. Among the various agrochemicals used globally, paraquat (N,N'-dimethyl-4, 4 -bipyridinium dichloride) is widely used as an herbicide due to its high water solubility and binding potential [1]. Recently, the presence of paraquat in waterbodies has been reported in different zones of the world [2]. Although paraquat is considered safe for many agricultural uses, thousands of deaths have occurred after paraquat ingestion (in humans often suicidal) or dermal exposure [3,4]. Therefore, paraquat removal from water sources is considered important.

The processes recommended for aqueous-phase removal of paraquat are grouped as destructive method (e.g., destructive oxidation) and recuperative method (e.g., adsorption) [5]. Compared with other methods, adsorption is superior due to its advantages such as easy operation, low cost, and higher efficiency for pesticide removal [6]. Adsorptive removal of paraquat from aqueous solution has been previously performed using adsorbents such as activated bleaching earth, laponite, goethite, waste coffee grounds, activated, and regenerated clay minerals [7–13]. Recently,

*Corresponding author.

batch adsorption study is used for the removal of metals from aqueous solution [14–16]. In all these previous studies, the performance of adsorbents has been investigated only for batch adsorption. Interestingly, continuous adsorption in packed bed is commercially worthwhile because the continuous contact between adsorbate and adsorbent allows for the efficient utilization of the adsorbent, thereby enhancing the treatment of the adsorbate solution [17].

In this study, rice husk ash (RHA) and bagasse fly ash (BFA), which are cheaply and commonly available biomass ashes, are used as adsorbents for the continuous removal of paraquat in packed column. The aim of the study was to evaluate and compare the performance of these two adsorbents for different influent concentrations, flow rates, and adsorbent loadings (dosages). The packed-bed parameters are determined and experimental results are analyzed using packed-bed models such as the bed depth service time, Thomas, and Yoon–Nelson models.

2. Materials and methods

2.1. Adsorbents

RHA was obtained from M/s Yash Agro Ltd, Nagpur (India) and BFA from M/s Wainganga Sugar and Power Ltd. Bhandara (India). The surface characteristics of these adsorbents such as surface area, pore diameter, and pore volume were measured using the BET surface area analyzer (ASAP 2010; Micromeritics, Germany). The chemical compositions of both the adsorbents were determined using XRF analyzer (PW 2403; PANalytical, the Netherlands) and elemental analyzer (vario MACRO Cube; Elementar, Germany). TEM micrographs were obtained from PHILIPS CM200 electron microscope. TGA analysis of RHA and BFA was performed with a heating rate of 5°C/min from 35 to 1000°C temperature using Perkin Elmer Diamond TG/DTA instrument.

2.2. Adsorbate

The adsorbate [paraquat (98%)] was purchased from Sigma Aldrich and used as such without any treatment. The chemical formula and molecular weight of paraquat are $C_{12}H_{14}Cl_2N_2$ and 257.16 g/mol, respectively. The stock solution of paraquat was prepared in deionized water and the solution was then diluted according to the experimental requirements.

2.3 Packed-bed adsorption

A glass column (1.2 cm internal diameter and 30 cm height) with four alternate openings at different positions from the bottom was fabricated for continuous removal of paraquat is shown in Fig. 1. According to the requirement for each experiment, the desired quantity of adsorbent (g) was packed between two supporting layers of glass wool. The purpose of using glass wool was to avoid the flow of adsorbent with effluent. To remove the entrapped air, deionized (~50 mL) water was pumped upward through the bed using a peristaltic pump (PP201 V; Electro Lab, India). Before performing the actual adsorption experiment, the column was kept inoperative for 12 h. The constant rate of influent solu-
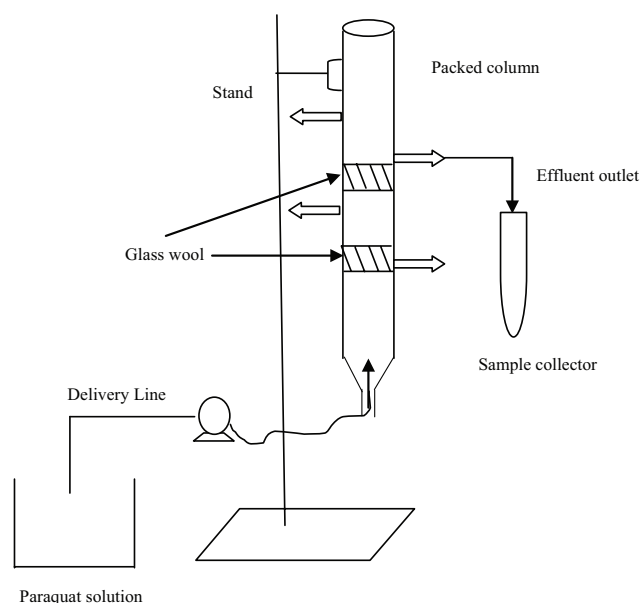
Fig. 1. Experimental setup of packed bed column.

tion was maintained using a rotameter mounted between the column and the pump. The effluent solution samples were collected periodically from the outlet, and the effluent concentration (C_t, mg/L) was analyzed on a UV–Vis spectrophotometer (Model UV 1800; Shimadzu, Japan) at 257 nm. Experiments were carried out for different influent concentrations (C_0), flow rates (Q), and bed heights (Z) at 30± 2°C (Table 1). Each experiment was performed in duplicate and average value was reported. Results were plotted in the form of breakthrough (BT) curves (C_t/C_0 Vs. time) for each experiment. The breakthrough (t_b or $t_{0.1}$) and saturation (t_s) points were assumed at $C_t/C_0 = 0.10$ and $C_t/C_0 = 0.98$ on BT curves, respectively.

2.4. Determination of packed-bed parameter

Packed-bed parameters such as bed capacity, length of the mass transfer zone (MTZ), fractional bed utilization (FBU), and percentage removal are important in determining the feasibility and economics of continuous adsorption process. The bed capacity at breakthrough point (Q_b mg/g) and bed capacity at saturation (Q_s mg/g) point were calculated as follows [17]:

$$Q_b = \frac{C_0 Q}{m} \int_0^{t_b} \left(1 - \frac{C_t}{C_0}\right) dt \tag{1}$$

$$Q_s = \frac{C_0 Q}{m} \int_0^{t_s} \left(1 - \frac{C_t}{C_0}\right) dt \tag{2}$$

where m (g) is the mass of adsorbent. The percentage removal was calculated from the quantity (mg) of paraquat entered and adsorbed in column. The length of mass transfer zone was obtained using Eq. (3)

$$MTZ = Z\left(1 - \frac{Q_b}{Q_s}\right) \tag{3}$$

Table1
Experimental condition for packed-bed adsorption of paraquat on RHA and BFA

Exp. No.	RHA			BFA		
	C_0 (mg/L)	Q (mL/min)	Z (cm)	C_0 (mg/L)	Q (mL/min)	Z (cm)
E1	10	5	6.4	10	5	4.4
E2	15	5	6.4	15	5	4.4
E3	20	5	6.4	20	5	4.4
E4	30	5	6.4	30	5	4.4
E5	20	2	6.4	20	2	4.4
E6	20	5	6.4	20	5	4.4
E7	20	7	6.4	20	7	4.4
E8	20	9	6.4	20	9	4.4
E9	20	5	3.2	20	5	3.0
E10	20	5	4.8	20	5	4.4
E11	20	5	6.4	20	5	6.0
E12	20	5	8.8	20	5	8.8

Table 2
Chemical composition of RHA and BFA (%)

	RHA	BFA
Al_2O_3	4.56	0.95
Fe_2O_3	1.58	1.62
MgO	0.63	1.96
MnO	052	1.15
CuO	0.18	0.12
CaO	1.27	3.62
K_2O	1.87	2.32
TiO_2	0.40	1.47
Na_2O	0.19	1.48

MTZ is important in calculating the FBU. The empty bed contact time (EBCT), that is, residence time, affects the behavior of BT curve and the volume of adsorbate treated. The EBCT (min) and adsorbent usage rate, U_r (g/mL), were calculated using Eqs. (4) and (5), respectively [18].

$$EBCT = \frac{V_c}{Q} = \frac{A_c Z}{Q} \qquad (4)$$

$$U_r = \frac{m}{V_b} = \frac{V_c \rho}{V_c N_b} \qquad (5)$$

where V_c (m³) is the adsorbent volume in bed, A_c (m²) is the cross-sectional area of column, V_b (m³) is the volume of adsorbate solution treated at breakthrough, ρ (g/cm³) is the apparent density of adsorbent, and N_b is the number of bed volumes of solution to breakthrough.

3. Results and discussion

3.1. Characterization of RHA and BFA

Proximate analysis of RHA and BFA was performed. In RHA, 1.80% moisture, 6.16% volatile matter, 89.87% ash and 2.17% fixed carbon whereas in BFA 6.30% moisture, 42.44% volatile matter, 40.16% ash and 11.10% fixed carbon content were found. The carbon percentage determined by CHNS analysis was 5.85% in RHA and 47.37% in BFA, whereas silica percentage identified by XRF analysis was 81.78% in RHA and 36.14% in BFA. Additionally, both the biomass ashes contain small quantities of metal oxides which play significant role in the adsorption process by forming charges on the surface of ash in aqueous solution. The metal oxides in RHA and BFA are presented in Table 3 which shows more content of Al_2O_3 in RHA and CaO in BFA. The BET surface area of RHA was measured to be 34 m²/g and that of BFA was 52 m²/g. The micropore area of RHA and BFA was 5.67 m²/g and 13.67 m²/g respectively.

The external surface area, determined using BET surface area and micropore area was found to be 28.32 m²/g and 38.26 m²/g for RHA and BFA respectively. The pore volume and pore diameter of RHA and BFA were 2.69 × 10⁻³ cm³/g and 4.96 × 10⁻² cm³/g and 80.60 Å and 45.58 Å, respectively, which suggests the existence of deeper pores on BFA and shallower pores on RHA surfaces.

The scanning electron micrographs (SEM) of RHA and BFA are shown in Fig. 2. The images in Fig. 2. indicate the ruptered, circular and elongated pores on the surface of both adsorbents. Some of the pores are internally connected. The aspect ratios in the range of 2.6:1 to 4.4:1 for BFA and 2.4:1 to 4.8:1 for RHA are earlier reported [19].

Transmission electron microscopy of RHA and BFA are shown in Fig. 3, we did not observe any regular pattern, which indicates the presence of amorphous zones throughout the matrix. The TEM images revealing the morphology and fiber distribution. It was also ascertained that the dark portion of the pictures are due to the homogenous dispersion of RHA and BFA.

The FTIR technique is an important tool to identify the characteristic functional groups on the adsorbent surface. The FTIR spectrum of RHA and BFA before and after paraquat adsorption are shown in Fig. 4. The FTIR spectrum of paraquat (Fig. 4a) shows characteristic peaks at 3053 and 3015 cm⁻¹, assigned to the C–H stretching mode of the terminal methyl groups on the aromatic ring in paraquat molecule. A set of weak bands between 1058 and 1216 cm⁻¹ assigned to the C–N vibrations for amines. 1360–1454 cm⁻¹ corresponds to C–H bending vibrations [20.]. The asymmetric C–H stretching occurs at slightly higher wave number as compared to that of symmetric C–H stretching. The C–H stretching of aromatic hydrocarbon obtains in the range from 3006–3053 cm⁻¹. The peak at 1277 indicates C–N stretching in aromatic amine and the bands from 2500–3000 cm⁻¹ arise due to methyl C–H stretching.

In Fig. 4c and 4e, the band 1667–2000 cm⁻¹ indicates the weak combinations and overtone absorption. The peaks in this region are assigned to mono to hexasubstitution of aromatic ring. The stretching of =C–H in aromatic compound is confirmed from the peak at 1614 cm⁻¹ for RHA. The bands in the region 1360–1380 cm⁻¹ are attributed to the aromatic C–H and carboxyl–carbonate structures. The peaks at 1080 cm⁻¹ in BFA and 1047 cm⁻¹ in RHA are the asymmetric stretching of Si–O–Si. The stretching vibration of Si–O at 667 cm⁻¹ is

Table 3
Packed-bed parameters for adsorption of paraquat using RHA and BFA under different conditions

Exp.No	EBCT (min)	t_{bexpt} (min)	t_s (min)	V_s (ml)	N_b	U_r (g/ml)	Q_b (mg/g)	Q_s (mg/g)	MTZ	FBU	% Removal
RHA											
E1	1.44	410	980	4900	105.65	0.002	4.07	5.98	2.03	0.68	61.05
E2	1.44	280	810	4050	72.15	0.003	4.17	6.45	2.25	0.64	53.08
E3	1.44	215	675	3375	55.40	0.004	4.21	6.68	2.36	0.63	49.48
E4	1.44	150	330	1650	38.65	0.006	4.40	7.20	2.48	0.61	72.72
E5	3.61	620	1190	2380	63.90	0.004	4.92	6.96	1.86	0.70	73.10
E6	1.44	215	675	3375	55.40	0.004	4.21	6.68	2.36	0.63	49.48
E7	1.03	150	420	2940	54.11	0.004	4.06	6.58	2.44	0.61	55.95
E8	0.80	110	235	2115	51.02	0.005	3.96	6.48	2.48	0.61	76.59
E9	0.72	85	325	1625	43.80	0.005	3.36	5.94	1.38	0.56	45.71
E10	1.08	145	410	2050	53.37	0.004	4.14	6.42	1.70	0.64	54.87
E11	1.44	215	675	3375	55.40	0.004	4.21	6.68	2.30	0.63	49.48
E12	1.98	320	780	3900	58.90	0.004	4.52	6.75	2.90	0.67	60.62
BFA											
E1	0.99	600	1320	6600	254.40	0.0008	11.20	14.40	0.97	0.77	54.54
E2	0.99	435	900	4500	184.44	0.0011	12.45	16.05	0.98	0.77	59.44
E3	0.99	330	690	3450	139.92	0.0015	12.60	16.38	1.01	0.77	59.26
E4	0.99	240	480	2400	101.76	0.0020	14.35	18.90	1.05	0.75	65.62
E5	2.48	830	1470	2940	140.76	0.0015	12.91	16.40	0.93	0.78	69.72
E6	0.99	330	690	3450	139.92	0.0015	12.60	16.35	1.01	0.77	59.26
E7	0.71	230	570	3990	136.52	0.0015	12.20	16.24	1.09	0.75	50.87
E8	0.55	165	450	4050	125.92	0.0016	11.37	15.98	1.26	0.71	49.33
E9	0.67	196	465	2325	138.50	0.0015	12.33	16.06	0.69	0.76	51.82
E10	0.99	330	690	3450	139.92	0.0015	12.60	16.35	1.01	0.77	59.26
E11	1.35	465	1020	5100	140.82	0.0015	12.85	16.57	1.34	0.77	56.86
E12	1.98	670	1560	7800	142.04	0.0014	13.05	20.55	3.20	0.63	65.86

(a)   (b)
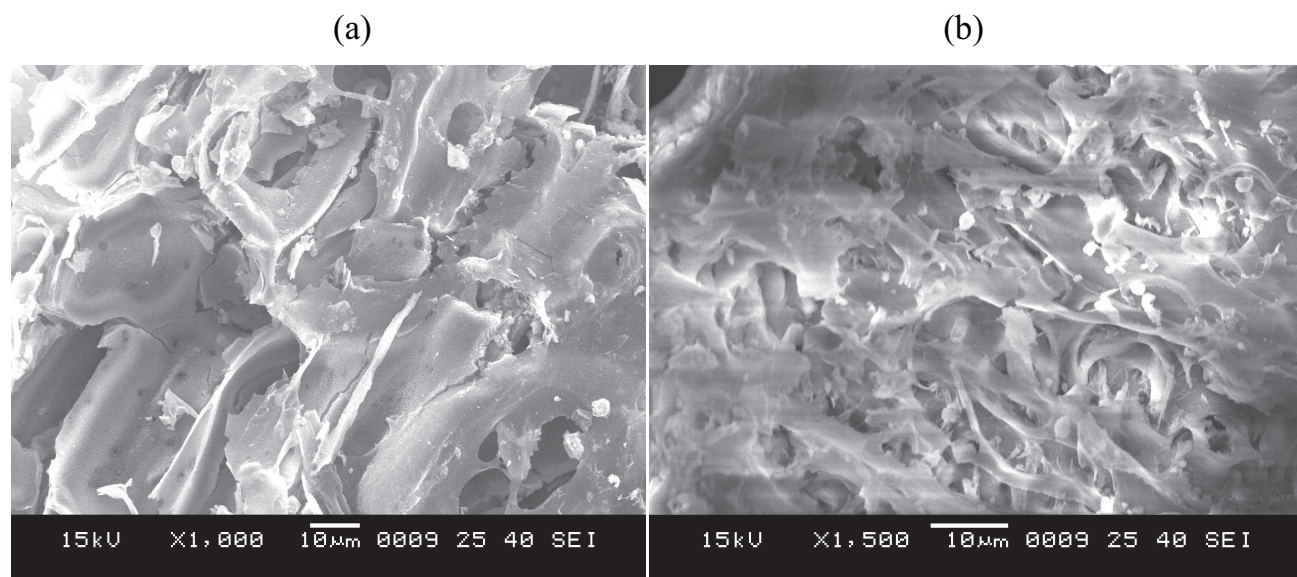
Fig. 2. Scanning electron micrographs of RHA (a) and BFA (b).

(a) (b)
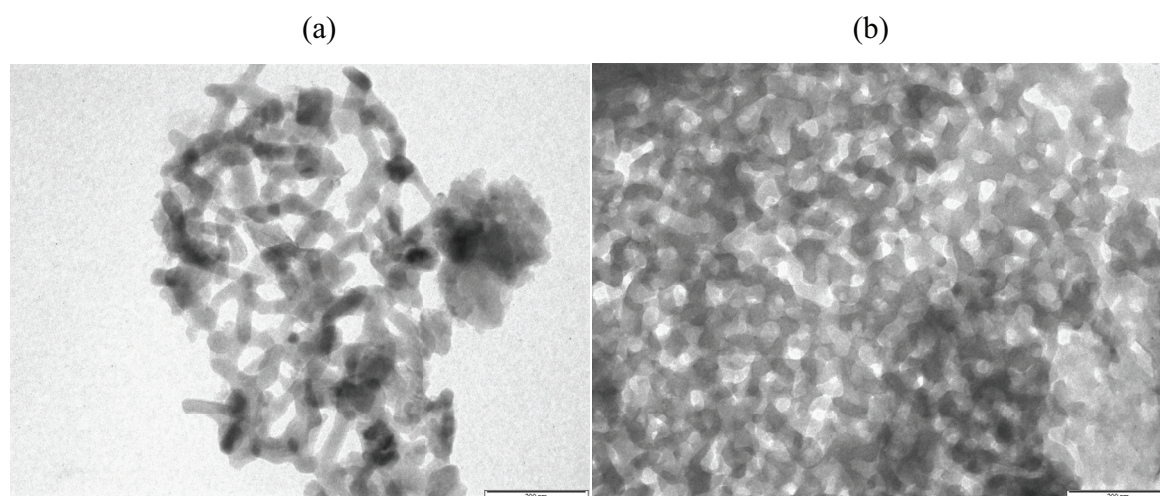
Fig. 3. Transmission electron microscopy of RHA (a) and BFA (b).

characteristic of quartz in BFA, whereas stretching vibration at 799 cm^{-1} in RHA corresponds to H–C bond. In BFA, the weak peak at 461 cm^{-1} is an indication of bending mode of internal tetrahedral (O–Si–O). In RHA, the peak at 469 cm^{-1} is due to the presence of Si–OH bond. In the BFA spectrum, the peaks at 1222 and 810 cm^{-1} are indicative of amorphous silica. The peaks around 1095 and 1134 cm^{-1} are indicative of a strong Si–O–Si stretch in polysiloxane or siloxanes. The presence of polar groups on the surface is likely to give considerable cation exchange capacity to RHA. [21].

FTIR spectrum of RHA and BFA after adsorption of paraquat (Fig. 4c and 4e) indicate the shifting of the bands. After adsorption of paraquat on RHA, peaks in Fig. 4d are observed at 1047 cm^{-1} and 2881 cm^{-1} related to the binding between the paraquat and RHA. This binding generates binary surface species, whose formation is mainly driven by electrostatic interactions. After adsorption of paraquat on BFA, Fig. 4b reveals new peaks at 1770, 1841, 2882 and 3078 cm^{-1}, which shows the binding between paraquat and BFA.

The above Figs. 5a and 5b show different trends in weight loss of RHA and BFA respectively as expected from their CHNS and XRF analysis. The overall weight loss observed was ~5% for RHA and ~45% for BFA. The initial minor weight loss near 100–250°C may be due to the removal of adsorbed water from both the ashes. For BFA the TGA curve shows a gradual weight loss from 200°C to 350°C followed by sharp weight loss from 350°C onward up to 1000°C which may be assigned to the volatile carboneous residue present in BFA. But for RHA after the initial moisture loss the major weight loss was registered from 250°C to 700°C. This may be due to volatile carbon residue which was very less compared to BFA. This observation may be supported by the CHNS and XRF composition of these two ashes. But after 700°C RHA did not show any weight loss indicating that the left over parts are inorganic oxides, which are thermally quite stable at this temperature region. [22].

3.2. Packed-bed parameters

The packed-bed parameters for adsorption of paraquat on RHA and BFA are listed in Table 3. EBCT in Table 3 varies
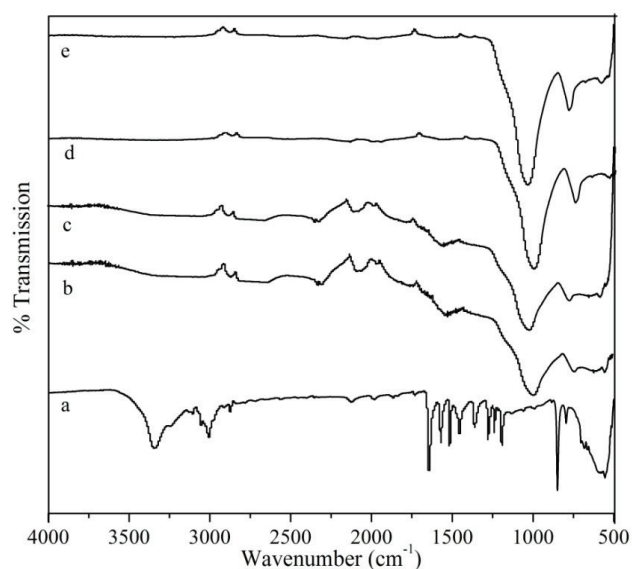
Fig. 4. FTIR Spectrum of (a) paraquat (b) BFA after adsorption (c) BFA (d) RHA after adsorption (e) RHA.

inversely with flow rate at a constant adsorbent dosage and varies directly with bed height at a constant flow rate. The bed capacities (Q_b and Q_s) of BFA are greater than those of RHA. In addition, the difference between Q_b and Q_s of each experiment for BFA is greater than that for RHA, which indicates the availability of more number of vacant sites after breakthrough time in BFA. The saturation of BFA bed occurred slowly, compared with RHA. Therefore, the volume (V_s) of adsorbate solution treated using BFA is larger than using RHA. The MTZ is greater in RHA than in BFA, whereas the fraction of bed utilization (FBU) is higher in BFA than in RHA, Thus, it can be recommended that greater the length of MTZ, higher the bed utilization. The percentage removal of paraquat for BFA is higher than for RHA. It can be observed that the saturation time of BFA bed is approximately 1.4 times higher than that of RHA bed and
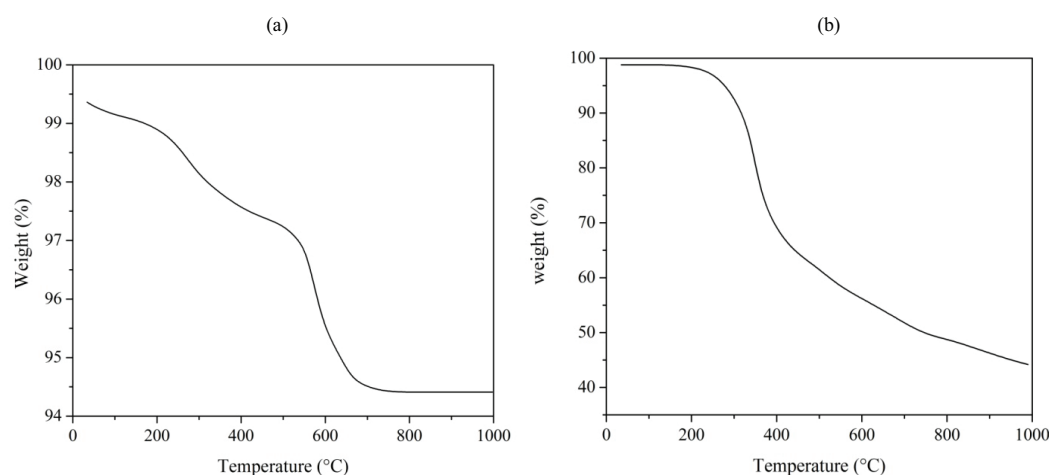
Fig. 5. Thermogravimetric analysis of RHA (a) and BFA (b).
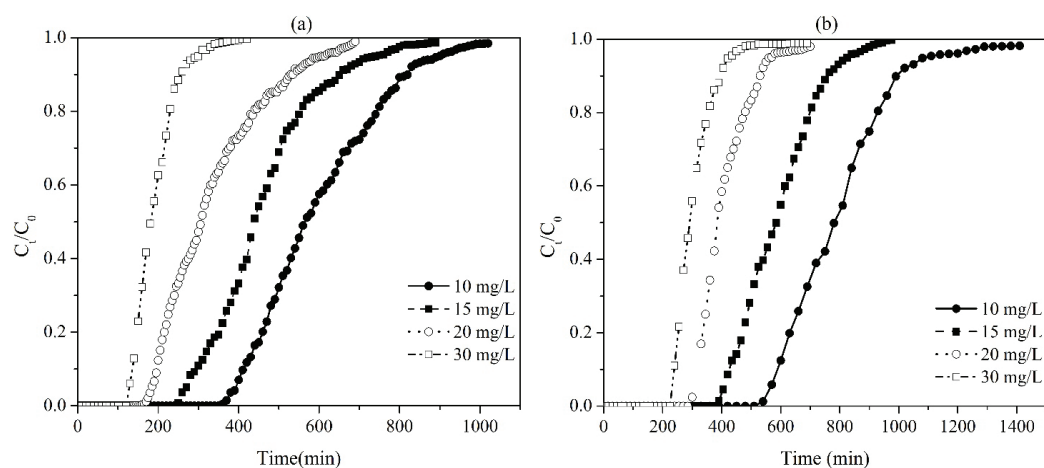
Fig. 6. Breakthrough curves for packed bed adsorption of paraquat (a) using RHA at Q = 5 mL/min, Z = 6.4 cm and (b) using BFA at Q = 5 mL/min, Z = 4.4 cm at different influent concentrations.

the capacity of BFA at saturation is about 2.8 times greater than that of RHA under the studied experimental conditions. The BFA usage rate (U_r) is comparatively lesser than RHA and this may be due to the higher surface area of BFA.

3.3. Effect of process parameters

3.3.1. Effect of influent concentration

The influent concentration of paraquat is varied between 10 and 30 mg/L at a constant flow rate and bed height for RHA and BFA. The results are plotted in the form of BT curves in Fig. 6, which indicate the early saturation of each adsorbent bed at higher influent concentration. This is due to the availability of finite adsorption sites for higher influent concentration. In addition, the activation energy at higher concentration is increased due to surface coverage of RHA and BFA, which makes further adsorption difficult [23]. The BT curves at higher influent concentrations became steeper because of reduced breakthrough time and saturation time (Table 3). The bed capacities (Q_b and Q_s) of both adsorbents are enhanced with increase in influent con-

centration. This is because of the gradient at higher influent concentration which offers a greater driving force for mass transfer [24]. The tailing of BT curves during the bed saturation of RHA as well as BFA can be observed in Fig. 6. This slow approach of BT curves is ascribed to the control of intraparticle diffusion over the mass transfer process [25]. For the same influent concentration, the breakthrough and saturation times, and the bed capacities are higher for BFA than for RHA. The enhancement in saturation capacity of BFA is greater than that of RHA for the same increase in influent concentration.

3.3.2. Effect of flow rate

The effect of flow rate on adsorption of paraquat was studied at a constant influent concentration and bed height by varying the flow rate 2 to 9 mL/min (Table 1). Results in Fig. 7 indicate steepest BT curves at 9 mL/min for RHA and elongated BT curves at 2 mL/min for BFA. The lower flow rate provides sufficient time for adsorbate molecules to penetrate the adsorbent pores, resulting in extended BT
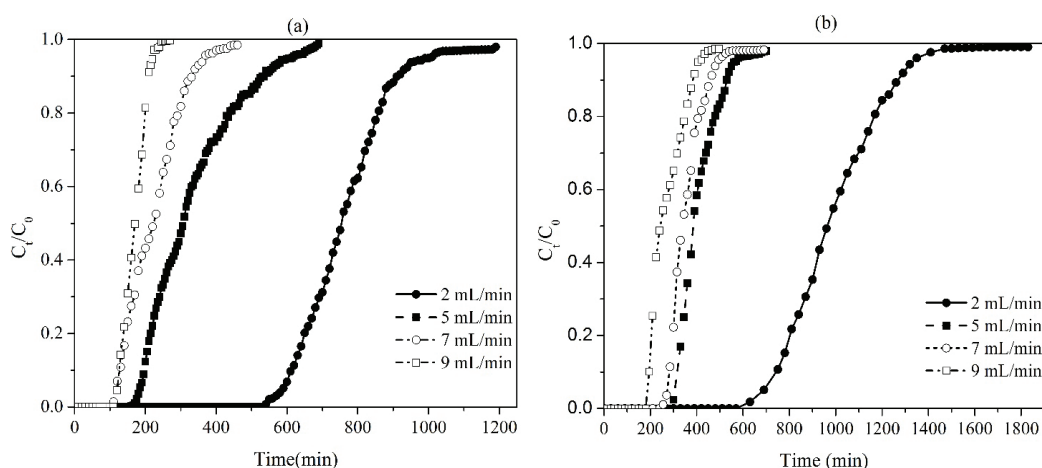
Fig. 7. Breakthrough curves for packed bed adsorption of paraquat (a) using RHA at C_0 = 20 mg/L, Z = 6.4 cm and (b) using BFA at C_0 = 20 mg/L, Z = 4.4 cm at different flow rates.
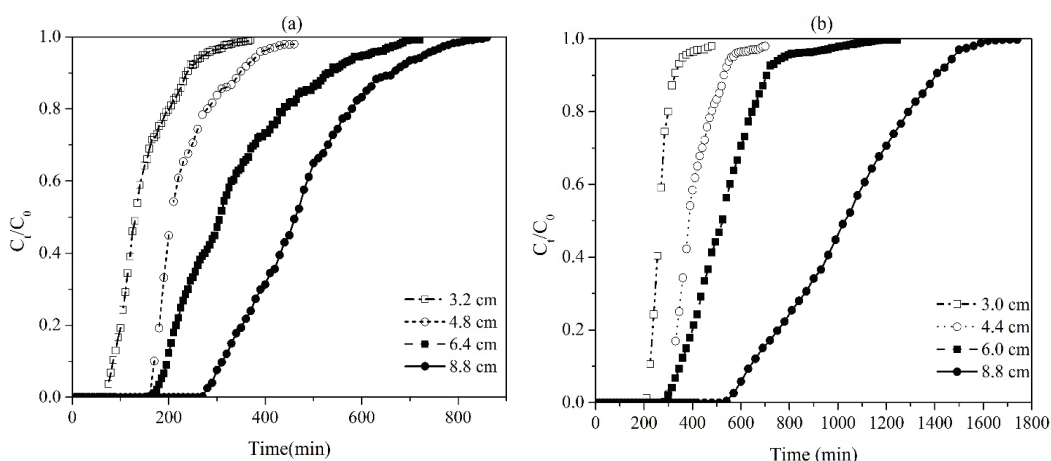
Fig. 8. Breakthrough curves for packed bed adsorption of paraquat (a) using RHA at C_0 = 20 mg/L, Q = 5 mL/min and (b) using BFA at C_0 = 20 mg/L, Q = 5 mL/min at different bed heights.

curves. With increasing flow rate, the breakthrough and saturation times, bed capacities, and percentage removal are considerably decreased (Table 3). Consequently, the volume of solution treated is also decreased with increase in flow rate. The diminution in capacity (Q_b or Q_s) and percentage removal at higher flow rate is ascribed to inadequate contact time, which results in early discharge of paraquat molecules from the adsorbent bed before the equilibrium is reached. With the increase in flow rate, the MTZ expands for both RHA and BFA, which causes an increase in mass transfer rate. Similar results were previously observed by Deokar et al. [26] in packed-bed adsorption of 2,4-D herbicide using bagasse fly ash. It can be deduced from Table 3 and Fig. 7 that the performance of RHA and BFA column is better at a lower flow rate than at a higher flow rate.

3.3.3. Effect of bed height

The bed height of RHA and BFA was changed according to experimental conditions in Table 1 at fixed influent concentration and flow rate. Fig. 8 shows that the BT curves

are extended for higher bed height (i.e., adsorbent loading) of RHA and BFA. The breakthrough and saturation times in Table 3 are significantly enhanced and thus the solution volume treated is also increased for higher bed height. The residence time of paraquat molecules in the RHA and BFA bed is higher for higher bed height as the molecules have to travel through a longer length of the bed. Therefore, the adsorbent bed needs more time for saturation, which results in extended BT curve. As the bed height is augmented, the surface area is increased and therefore the bed capacities of both adsorbents are also increased [27]. Because of higher breakthrough and saturation capacities, the length of MTZ is significantly increased with increase in bed height. However, the utilization of RHA and BFA bed is reduced with increase in bed height. The bed capacity is less for lower bed height and this may be due to a shorter time needed for diffusion of paraquat molecules into the adsorbent bed. Therefore, beds of increased height may be suggested for better column performance. Similar results for variable bed height have been previously reported for packed-bed adsorption of phenoxyacetic acid herbicide [28].

3.4. Application of packed-bed models

3.4.1. Modeling of column adsorption data

Successful design of a column for continuous adsorption in a packed bed demands the estimation of the concentration–time profile from the BT curves. To predict and analyze the dynamic behavior of paraquat adsorption onto RHA and BFA, various models including the BDST, Thomas, and Yoon–Nelson models were applied to the experimental data [29]. To judge the best-fit model, error analysis [17] was performed by considering standard deviation (ε) and Marquardt's percent standard deviation (MPSD) between the experimental and predicted data.

$$MPSD = 100 \times \sqrt{\frac{1}{N-P}\Sigma\left(\frac{\left(\frac{C_t}{C_0}\right)_{expt} - \left(\frac{C_t}{C_0}\right)_{pred}}{\left(\frac{C_t}{C_0}\right)_{expt}}\right)^2} \qquad (6)$$

$$\varepsilon = 100 \times \left(\frac{t_{b\,expt} - t_{bpred}}{t_{b\,expt}}\right) \qquad (7)$$

3.4.1. Application of the bed depth service time model

The BDST model considers negligible intraparticle diffusion and external mass transfer resistance [30,31]. The model assumes that the adsorption is limited by surface reaction between adsorbate and unused capacity of adsorbent [23]. It is given by the following equation:

$$t = \frac{N_0}{C_0 u_0}Z - \frac{1}{C_0 K_{BD}}\ln\left(\frac{C_0}{C_t} - 1\right) \qquad (8)$$

where N_0 is the adsorption capacity of bed (mg/L), U_0 (cm/min) is a linear flow velocity, and K_{BD} is the rate constant (L/mg·min). The BDST model (t vs. Z) is shown in Fig. 9 for packed-bed adsorption of paraquat on RHA and BFA. The values of model parameters are determined for 10, 50,

and 90% BT at constant concentration and flow rate, and are presented in Table 4.

The adsorption capacity (N_0 mg/L) is found to be 3457, 5296 and 6976 for RHA, and 6292, 11721, 16185 for BFA at 10, 50, and 90% BT, respectively. The BFA capacity (90% BT) predicted by the BDST model is approximately 2.3 times greater than that of RHA. The rate constant (K_{BD}, L/mg·min) determined from intercept is 5.7×10^{-4} for RHA and 9.3×10^{-4} for BFA at 10% BT of column. The values of coefficient of determination (R^2) as shown in Fig. 9 are close to one, which indicates the fitting of the BDST model for experimental data. The linear lines in Fig. 9 for 10, 50, and 90% BT are not parallel, which is due to the dissimilar lengths of MTZ. This informs that the MTZ in RHA and BFA bed does not move with constant velocity during packed-bed adsorption of paraquat. The probable reason may be the insufficient bed height to develop constant pattern behaviour [32]. In this study, the linear line representing 50% BT for RHA and BFA intercepts the y axis, but in an ideal scenario, this line should pass through the origin. Therefore, according to the BDST model, adsorptive removal of paraquat on RHA and BFA is controlled by a complex mechanism comprising more than one rate-limiting step [18].

3.4.3. Application of the Thomas model

The Thomas model is applied to the experimental data between (C_t/C_0) = 0.01 and 0.98, and maximum solid-phase concentration and adsorption rate of paraquat are determined for RHA and BFA. The linear form of the Thomas model [33] is expressed as follows:

$$\ln\left(\frac{C_0}{C_t} - 1\right) = \frac{K_T Q_0 m}{Q} - K_T C_0 t \qquad (9)$$

The kinetic constant K_T [L/(mg min)] and adsorption capacity Q_0 (mg/g) for the Thomas model are calculated from slope and intercept of Eq. (9), respectively. These values are presented in Table 4 for different experimental condition. The Thomas model adsorption capacity of BFA is appreciably higher than that of RHA. The adsorption capac-
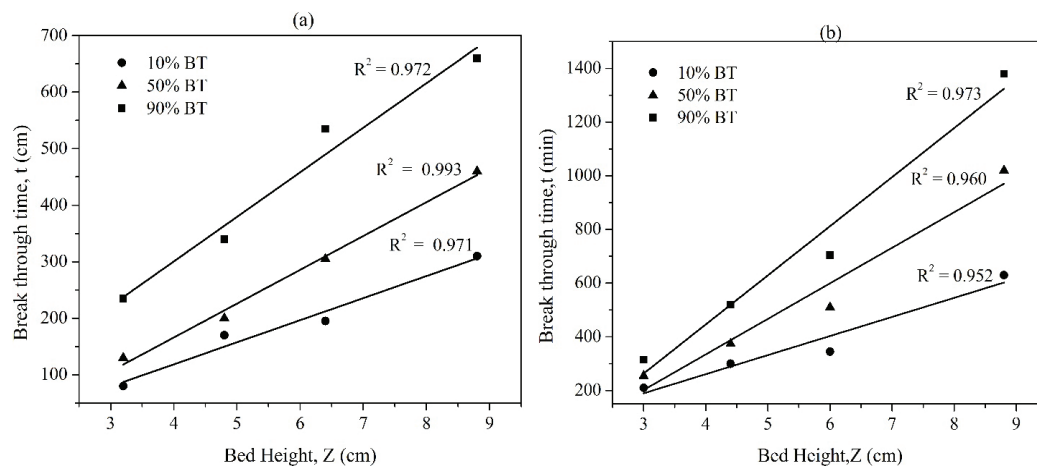
Fig. 9. Bed depth service time model for adsorption of paraquat on (a) RHA and (b) BFA at different bed heights and constant concentration (20 mg/L) and flow rate (5 mL/min).

Table 4
Parameters of packed-bed models for adsorption of paraquat on RHA and BFA

Exp.	Thomas model					Yoon–Nelson model				
	K_T (L/(mg min))	q_0 (mg/g)	t_{bpred} (min)	ε	MPSD	K_{YN} (min^{-1})	$t_{0.5}$expt (min)	t_{bpred} (min)	ε	MPSD
	RHA									
E1	0.53×10^{-3}	9.62	380	7.31	32.20	10.3×10^{-3}	560	596	−6.49	32.20
E2	0.54×10^{-3}	9.87	270	3.57	25.17	11.5×10^{-3}	430	464	−7.87	25.16
E3	0.55×10^{-3}	9.99	125	41.86	49.05	11.0×10^{-3}	305	328	−7.38	49.05
E4	0.88×10^{-3}	10.13	90	40.00	8.20	26.5×10^{-3}	180	182	−1.20	8.20
E5	0.58×10^{-3}	10.25	580	6.45	48.09	11.7×10^{-3}	750	769	−2.53	48.09
E6	0.55×10^{-3}	9.99	125	41.86	49.05	11.0×10^{-3}	305	328	−7.38	49.05
E7	0.35×10^{-3}	9.80	110	26.66	88.73	20.5×10^{-3}	220	226	−2.77	88.69
E8	0.29×10^{-3}	8.68	130	-18.18	19.28	55.8×10^{-3}	170	168	1.09	16.01
E9	0.19×10^{-3}	8.76	55	35.29	55.52	23.8×10^{-3}	130	148	−13.84	55.52
E10	0.34×10^{-3}	9.60	70	51.72	20.69	16.9×10^{-3}	200	209	−4.50	21.47
E11	0.55×10^{-3}	9.99	125	41.86	49.05	11.0×10^{-3}	305	328	−7.38	49.05
E12	0.62×10^{-3}	10.36	100	68.75	37.22	12.4×10^{-3}	460	476	−3.43	36.99
	BFA									
E1	0.93×10^{-3}	16.04	540	10.00	114.37	9.3×10^{-3}	780	802	−2.86	114.37
E2	0.87×10^{-3}	17.76	420	3.44	65.86	13.1×10^{-3}	585	592	−1.22	65.78
E3	0.81×10^{-3}	17.82	225	31.81	17.19	14.2×10^{-3}	375	386	−2.95	17.19
E4	0.78×10^{-3}	18.02	195	18.75	22.87	23.4×10^{-3}	285	300	−5.43	22.87
E5	0.43×10^{-3}	15.91	690	16.86	28.04	8.7×10^{-3}	960	995	−3.60	57.56
E6	0.71×10^{-3}	15.44	225	31.81	17.19	15.4×10^{-3}	375	402	−7.23	107.21
E7	0.97×10^{-3}	15.22	220	4.34	62.20	22.1×10^{-3}	330	357	−8.07	63.62
E8	0.99×10^{-3}	14.83	150	9.09	26.61	19.9×10^{-3}	240	266	−10.76	26.61
E9	1.23×10^{-3}	16.98	195	0.51	30.19	24.7×10^{-3}	255	255	0.08	23.50
E10	0.71×10^{-3}	17.74	225	31.81	17.19	15.4×10^{-3}	375	402	−7.23	107.21
E11	0.49×10^{-3}	18.75	315	32.25	50.90	9.9×10^{-3}	510	538	−5.46	52.48
E12	0.30×10^{-3}	20.41	660	1.49	24.41	6.1×10^{-3}	1020	1021	−0.08	25.70

ity of RHA and BFA (Table 4) is enhanced by the increase in influent concentration and bed height owing to increase in concentration gradient and adsorption sites, respectively. However, this capacity is reduced for increased flow rate. A similar change in capacity with change in concentration, flow rate, and bed height was previously reported by Deokar et al. [17]. It can be observed from Table 4 that the kinetic constant for both the adsorbents is a function of influent concentration, flow rate, and bed height. The breakthrough time (t_{bpred}, Table 4) predicted by the Thomas model is compared with the experimental value ((t_{bexpt}, Table 3) and standard percent deviation (ε) is calculated (Table 4). For most of the experiments, the greater deviation (higher value of ε) between the experimental and predicted values of breakthrough times was observed (Table 4), may be because the Thomas model is based on second-order reaction kinetics, whereas adsorption is governed by both chemical reaction kinetics and interphase mass transfer [34]. The MPSD values for the Thomas model shows that the experimental and predicted values of (C_t/C_0) are closer and therefore, the experimental BT curves and the corresponding predicted BT curves for each adsorbent in Fig. 10a and 10b are similar.

The fitting of the Thomas model for adsorption of paraquat on RHA and BFA implies that external and internal diffusions are not the only rate-limiting steps [35].

3.4.4. Application of the Yoon–Nelson model

The Yoon–Nelson model does not require the detailed information about the type and properties of adsorbent and properties of the bed [25]. This model predicts the time ($t_{0.5}$) necessary for 50% saturation of adsorbent bed [36]. In this study, the Yoon–Nelson model [Eq. (10)] is applied to the data in the range $0.01 < (C_t/C_0) < 0.98$, and the model parameters are calculated from slope and intercept

$$\ln\left(\frac{C_t}{C_0 - C_t}\right) = K_{YN}t - t_{0.5}K_{YN} \tag{10}$$

where K_{YN} is the kinetic constant (min^{-1}), $t_{0.5}$ is predicted or the time required for 50% adsorbate breakthrough (min), and t is the breakthrough (sampling) time (min). The parameters of the Yoon–Nelson model for paraquat adsorption on RHA and BFA are listed in Table 4. In most of the
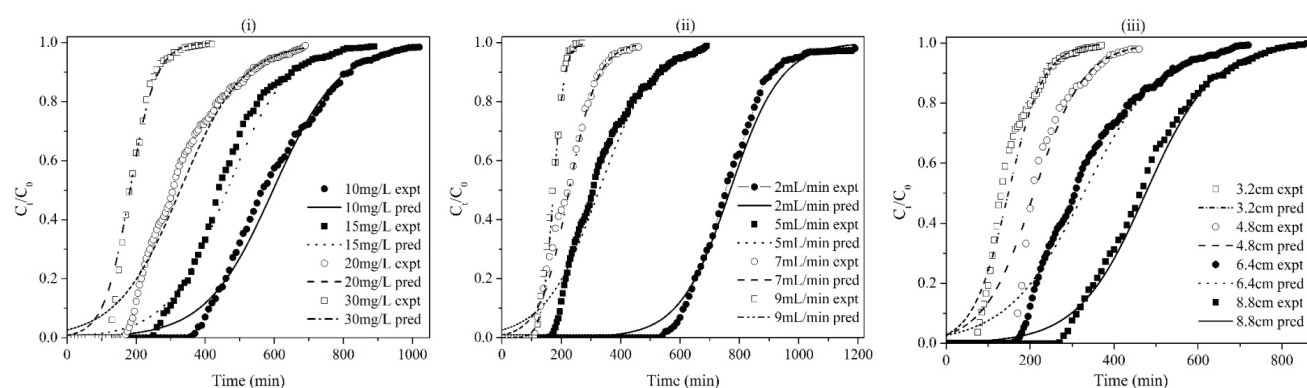
Fig. 10a. Comparison between experimental and predicted breakthrough curves for packed-bed adsorption of paraquat on RHA using the Thomas model: (i) Q = 5 mL/min, Z = 6.4 cm; (ii) C_0 = 20 mg/L, Z = 6.4 cm; (iii) C_0 = 20 mg/L, Q = 5 mL/min.
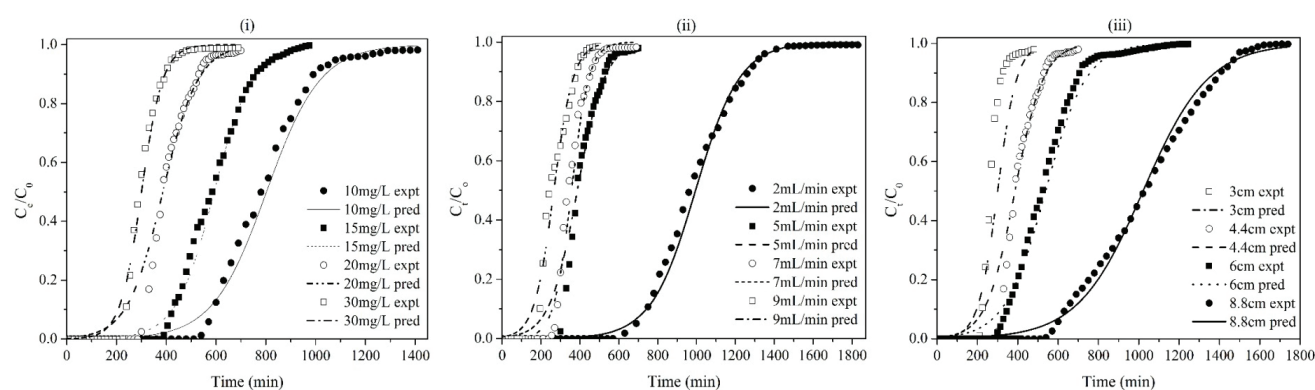
Fig. 10b. Comparison between experimental and predicted breakthrough curves for packed-bed adsorption of paraquat on BFA using the Thomas model: (i) Q = 5 mL/min, Z = 4.4 cm; (ii) C_0 =20 mg/L, Z = 4.4 cm; (iii) C_0 = 20 mg/L, Q = 5 mL/min.
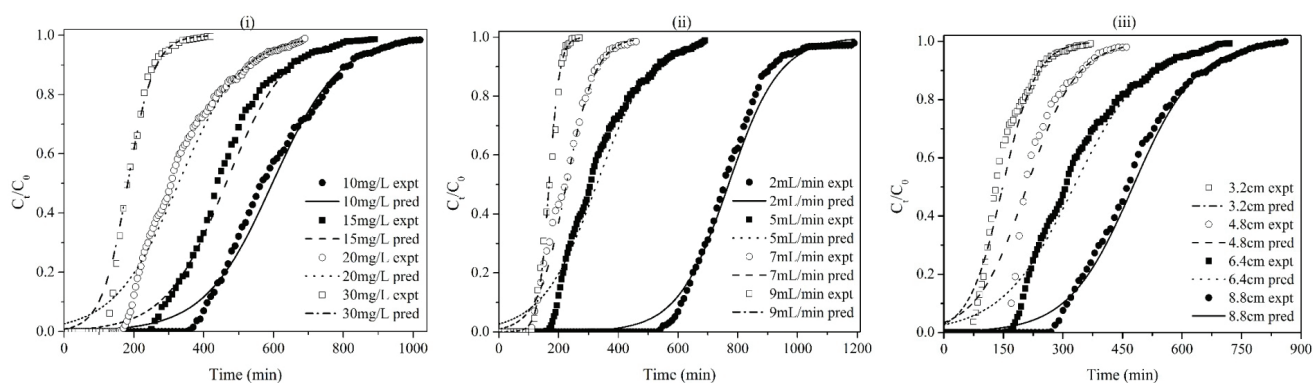
Fig. 11a. Comparison between experimental and predicted breakthrough curves for packed-bed adsorption of paraquat on RHA using the Yoon–Nelson model: (i) Q = 5 mL/min, Z = 6.4 cm; (ii) C_0 = 20 mg/L, Z = 6.4 cm; (iii) C_0 = 20 mg/L, Q = 5 mL/min.

experiments, the predicted time ($t_{0.5pred}$) for 50% saturation is greater than experimental time ($t_{0.5expt}$). The intraparticle diffusion after 50% saturation of bed forms nonsymmetrical BT curves, indicating delay in saturation time [37]. This results in higher predicted 50% breakthrough time than that obtained in the experiments. The experimental BT curves are compared with the curves predicted by the Yoon–Nelson model in Fig.11a and Fig.11b. As indicated in Fig. 11a

and Fig.11b, the fitting of the Yoon–Nelson model is more appropriate for the paraquat adsorption on both adsorbents. This observation can be verified from the values of deviations (MPSD, ε), which are lower for the Yoon–Nelson model than for the Thomas model. Therefore, the predicted time for 50% saturation is in close accordance with the experimental time for adsorption of paraquat on RHA and BFA.
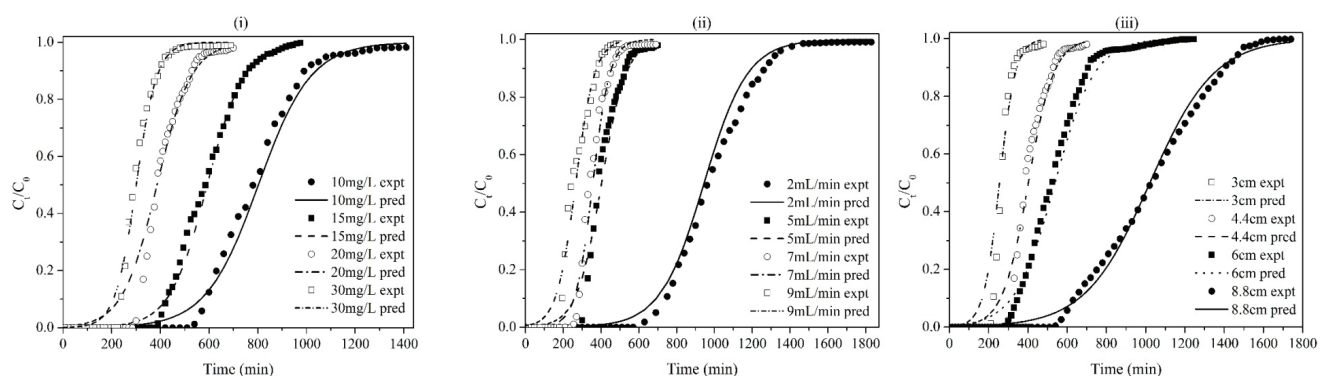
Fig. 11b. Comparison between experimental and predicted breakthrough curves for packed-bed adsorption of paraquat on BFA using the Yoon–Nelson model: (i) Q = 5 mL/min, Z = 4.4 cm; (ii) C_0 = 20 mg/L, Z = 4.4 cm; (iii) C_0 = 20 mg/L, Q = 5 mL/min.

Table 5
Comparison of adsorption efficacy of activated carbon with that of RHA and BFA

Adsorbent	q_{cap} (mg/g)	Surface area (m^2/g)	$q_{cap} \times 10^3$ (mg/m^2)	Ref No.
Activated bleaching Earth	26.74	268	99.77	[7]
Commercial activated carbon	75.8	1050	72.19	[38]
Tires activated carbon	33.7	832	40.50	
Activated clay	0.06	266	0.22	[11]
	0.05	270	0.18	
	0.04	230	0.17	
Regenerated clay mineral	1.31	101.5	12.90	[12]
BFA	20.55	52	395.2	This study
RHA	6.96	34	204.70	This study

3.5. Comparison between different paraquat adsorbents

Table 5 presents a comparison of adsorption capacity of various adsorbents for paraquat removal. The adsorption capacities in this table are reported as (i) the quantity of adsorbate adsorbed (mg) per unit mass (g) of the adsorbent and (ii) the quantity of adsorbate adsorbed (mg) per unit surface area (m^2) of the adsorbent. Compared with natural (neither chemically modified nor laboratory synthesized), low-cost, and soil-compatible adsorbents, BFA has the highest adsorption capacity (mg/m^2) for paraquat removal. This indicates that the studied biomass ashes (i.e. RHA and BFA) are the most efficient adsorbents for the removal of paraquat from aqueous solution.

4. Conclusions

Adsorptive removal of paraquat is performed in packed bed of RHA and BFA at different experimental conditions such as influent concentrations, flow rates, and bed heights. The packed-bed parameters, especially adsorbent capacity, fraction of bed utilization, adsorbent usage rate, empty bed contact time, length of MTZ, volume of solution treated, and breakthrough and saturation times are noticeably influenced by the change in experimental conditions. Both RHA and BFA have maximum adsorption capacity at a higher influent concentration and bed height, and at a lower flow rate. In comparison with RHA, BFA has higher value of adsorption capacity, bed utilization, and percentage removal.

The BDST, Thomas, and Yoon–Nelson models are applied to packed-bed data. The BDST model reveals the complex mechanism involving more than one rate-controlling step in the adsorption of paraquat using RHA and BFA. The BDST model implies that BFA has 2.3 times higher capacity than RHA. The Yoon–Nelson model is better than the Thomas model because the deviations between experimental and predicted values are lesser for the former model.

References

[1] M. Brigante, P.C. Schulz, Adsorption of paraquat on mesoporous silica modified with titania: Effects of pH, ionic strength and temperature, J. Colloid Interface Sci., 363 (2011) 355–361.
[2] M.S.F. Santos, G. Schaule, A. Alves, L.M. Madeira, Adsorption of paraquat herbicide on deposits from drinking water networks, Chem. Eng. J., 229 (2013) 324–333.
[3] W.T. Tsai, H.R. Chen, Adsorption kinetics of herbicide paraquat in aqueous solution onto a low-cost adsorbent, swine-manure-derived biochar, Int. J. Environ. Sci. Technol., 10 (2013) 1349–1356.
[4] K.M. Ibrahim, H.A. Jbara, Removal of paraquat from synthetic wastewater using phillip site–faujasite tuff from Jordan, J. Hazard. Mater., 163(1) (2009) 82–86.
[5] W.T. Tsai, C.W. Lai, K.J. Hsien, Adsorption kinetics of herbicide paraquat from aqueous solution onto activated bleaching earth, Chemosphere, 55(2004) 829–837.

[6] S.K. Deokar, G.S. Bajad, P. Bhonde, R.P. Vijayakumar, S.A. Mandavgane, Adsorptive removal of diuron herbicide on carbon nanotubes synthesized from plastic waste, J. Polym. Environ., (2016) 1–11.

[7] W.T. Tsai, M.F. Hsieh, H.F. Sun, S. F. Chien, H. P. Chen, Adsorption of paraquat onto activated bleaching earth, Bull Environ. Contam. Toxicol., 69 (2002) 189–194.

[8] K. Esumi, Y. Takeda, Y. Koide, Competitive adsorption of cationic surfactant and pesticide on laponite, Colloids Surf. A., 135 (1998) 59–62.

[9] M. Brigante, G. Zanini, M. Avena, Effect of humic acids on the adsorption of paraquat by goethite, J. Hazard. Mater., 184 (2010) 241–247.

[10] K.C. Kemp, S.B. Baek, W.G. Lee, M. Meyyappan, K.S. Kim, Activated carbon derived from waste coffee grounds for stable methane storage, Nanotechnology, 26 (2015) 1–8.

[11] W.T. Tsai, C.W. Lai, K.J. Hsien, Effect of particle size of activated clay on the adsorption of paraquat from aqueous solution, J. Colloid. Interface. Sci., 263(2003) 29–34.

[12] W.T. Tsai, C.W. Lai, Adsorption of herbicide paraquat by clay mineral regenerated from spent bleaching earth, J. Hazard. Mater. B., 134 (2006) 144–148.

[13] Y. Seki, K. Yurdakoc, Paraquat adsorption onto clays and organoclays from aqueous solution, J. Colloid. Interface. Sci., 287 (2005) 1–5.

[14] Z.Z. Chowdhury, W.A. Yehye, N.M. Julkapli, M.A.H. AlSaadi, M.A. Atieh, Application of graphitic bio-carbon using two-level factorial design for microwave-assisted carbonization, BioResources, 11(2) (2016) 3637–3659.

[15] G.A. Adebisi, Z.Z. Chowdhury, S.B.A. Hamid, E. Ali, Hydrothermally treated banana empty fruit bunch fiber activated carbon for Pb(II) and Zn(II) removal, BioResources, 11(4) (2016) 9686–9709.

[16] Z.Z. Chowdhury, S.A. Hamid, M.M. Rahman, R.F. Rafique, Catalytic activation and application of micro-spherical carbon derived from hydrothermal carbonization of lingo cellulosic biomass: statistical analysis using Box–Behnken design, RSC Advances, 6(104) (2016) 102680–102694.

[17] S.K. Deokar, S.A. Mandavgane, Estimation of packed bed parameters and prediction of breakthrough curves for adsorptive removal of 2, 4-dichloro phenoxy acetic acid using rice husk ash, J. Environ. Chem. Eng., 3 (2015) 1827–1836.

[18] V.C. Srivastava, B. Prasad, I.M. Mishra, I.D. Mall, M.M. Swamy, Prediction of breakthrough curves for sorptive removal of phenol by bagasse fly ash packed bed, Ind. Eng. Chem. Res., 47(5) (2008) 1603–1613.

[19] S.K. Deokar, S.A. Mandavgane, B.D. Kulkarni, Comparative evaluation of packed-bed performance of biomass ashes as adsorbents for removal of diuron from aqueous solution, Desal. Water Treat., 57(59) (2016) 28831–28846.

[20] M. Brigante, M. Avena, Synthesis, characterization and application of a hexagonal mesoporous silica for pesticide removal from aqueous solution, Micropor. Mesopor. Mater., 191 (2014) 1–9.

[21] S.K. Deokar, S.A. Mandavgane, B.D. Kulkarni, Behaviour of biomass multicomponent ashes as adsorbents, Current Sci., 110 (2016) 180–186.

[22] M. Tsukada, H. Yamada, H. Kamiya, Analysis of biomass combustion ash behavior at elevated temperatures, Adv. Powder Technol., 14(6) (2003) 707–717.

[23] R. Han, Y. Wang, X. Zhao, Y. Wang, F. Xie, J. Cheng, M. Tang, Adsorption of methylene blue by phoenix tree leaf powder in a fixed-bed column: experiments and prediction of breakthrough curves, Desalination, 245 (2009) 284–297.

[24] S. Sadaf, H.N. Bhatti, Evaluation of peanut husk as a novel, low cost biosorbent for the removal of Indosol Orange RSN dye from aqueous solutions: batch and fixed bed studies, Clean Techn. Environ. Policy, 16 (2014) 527–544.

[25] R. Han, Y. Wang, W. Yu, W. Zou, J. Shi, H. Liu, Biosorption of methylene blue from aqueous solution by rice husk in a fixed-bed column, J. Hazard. Mater., 141 (2007) 713–718.

[26] S.K. Deokar, S.A. Mandavgane, B.D. Kulkarni, Adsorptive removal of 2, 4-dichloro phenoxy acetic acid from aqueous solution using bagasse fly ash as adsorbent in batch and packed-bed techniques, Clean Techno. Environ. Policy, 18 (2016) 1971–1983.

[27] C. Sukumar, V. Janaki, K. Vijayaraghavan, S.K. Kannan, K. Shanthi, Removal of Cr(VI) using co-immobilized activated carbon and Bacillus subtilis: fixed-bed column study, Clean Techn. Environ. Policy, (2016) 1–8. DOI 10.1007/s10098-016-1203-2.

[28] S.K. Deokar, S.A. Mandavgane, B.D. Kulkarni, Agro-industrial waste: a low cost adsorbent for effective removal of 4-chloro-2-methylphenoxyacetic acid herbicide in batch and packed bed modes, Environ. Sci. Pollut. Res., 23 (2016) 16164–16175.

[29] C.B. Lopes, E. Pereira, Z. Lin, P. Pato, M. Otero, C.M. Silva, A.C. Duarte, Fixed-bed removal of Hg^{2+} from contaminated water by microporous titano silicate ETS-4: Experimental and theoretical breakthrough curves, Micropor. Mesopor. Mater., 145 (2011) 32–40.

[30] M. Jahangiri-rad, A. Jamshidi, M. Rafiee, R. Nabizadeh, Adsorption performance of packed bed column for nitrate removal using PAN-oxime-nanoFe$_2$O$_3$, J. Environ. Health Sci. Eng., 12(1) (2014) 1–5.

[31] P.V. Nidheesh, R. Gandhimathi, S.T. Ramesh, T.S.A. Singh, Adsorption and desorption characteristics of crystal violet in bottom ash column, J. Urban Environ. Eng., 6(1) (2012) 18–29.

[32] J.L. Sotelo, A. Rodrıguez, S.A. lvarez, J. Garcia, Removal of caffeine and diclofenac on activated carbon in fixed bed column, Chem. Eng. Res. Des., 90 (2012) 967–974.

[33] C.E. Rodriguez-Martinez, Z.I. Gonzalez-Acevedo, M.T. Olguın, H. Frias-Palos, Adsorption and desorption of selenium by two non-living biomasses of aquatic weeds at dynamic conditions, Clean Techn. Environ. Policy, 18 (2016) 33–44.

[34] B. Preetha, T. Viruthagiri, Batch and continuous biosorption of chromium(VI) by Rhizopusarrhizus, Sep. Purif. Technol., 57 (2007) 126–133.

[35] Z. Aksu, F. Gonen, Biosorption of phenol by immobilized activated sludge in a continuous packed bed: Prediction of breakthrough curves, Process Biochem., 39 (2004) 599–613.

[36] Z.Z. Chowdhury, S.B.A. Hamid, S.M. Zain, Evaluating design parameters for breakthrough curve analysis and kinetics of fixed bed columns for Cu (II) cations using lignocellulosic wastes, BioResources, 10(1) (2014) 732–749.

[37] A.S.A. Aziz, L.A. Manaf, H.C. Man, N.S. Kumar, Column dynamic studies and breakthrough curve analysis for Cd(II) and Cu(II) ions adsorption onto palm oil boiler mill fly ash (POFA), Environ. Sci. Pollut. Res., 21 (2014) 7996–8005.

[38] N.K. Hamadi, S. Swaminathan, X.D. Chen, Adsorption of paraquat dichloride from aqueous solution by activated carbon derived from used tires, J. Hazard. Mater., 112 (2004) 133–141.